HHS Public Access

Author manuscript

Biomaterials. Author manuscript; available in PMC 2017 May 01.

Published in final edited form as:

Biomaterials. 2016 May ; 88: 25–33. doi:10.1016/j.biomaterials.2016.02.021.

Transcatheter Intra-Arterial Infusion of Doxorubicin Loaded Porous Magnetic Nano-clusters with Iodinated Oil for the Treatment of Liver Cancer

Min Jeong Jeon[a,1], **Andrew C. Gordon**[b,d,1], **Andrew C. Larson**[b,c,d,e,f], **Jin Wook Chung**[a], **Young Il Kim**[a,g,*], and **Dong-Hyun Kim**[b,c,**]

Young Il Kim: ykimphd@gmail.com; Dong-Hyun Kim: dhkim@northwestern.edu

[a]Department of Radiology, Seoul National University Hospital, Seoul, Korea

[b]Department of Radiology, Northwestern University, Chicago, IL, USA

[c]Robert H. Lurie Comprehensive Cancer Center, Chicago, IL, USA

[d]Department of Biomedical Engineering, Northwestern University, Evanston, IL, USA

[e]Department of Electrical Engineering and Computer Science, Evanston, IL, USA

[f]International Institute of Nanotechnology (IIN), Northwestern University, Evanston, IL, USA

[g]Department of Radiology, Sheikh Khalifa Specialty Hospital, Ras Al Khaimah, United Arab Emirates

Abstract

A promising strategy for liver cancer treatment is to deliver chemotherapeutic agents with multifunctional carriers into the tumor tissue via intra-arterial (IA) transcatheter infusion. These carriers should release drugs within the target tissue for prolonged periods and permit intra-procedural multi-modal imaging of selective tumor delivery. This targeted transcatheter delivery approach is enabled via the arterial blood supply to liver tumors and utilized in current clinical practice which is called chemoembolization or radioembolization. During our study, we developed Doxorubicin (Dox) loaded porous magnetic nano-clusters (Dox-pMNCs). The porous structure and carboxylic groups on the MNCs achieved high-drug loading efficiency and sustained drug release, along with magnetic properties resulting in high MRI T2-weighted image contrast. Dox-pMNC within iodinated oil, Dox-pMNCs, and Dox within iodinated oil were infused via hepatic arteries to target liver tumors in a rabbit model. MRI and histological evaluations revealed that the long-term drug release and retention of Dox-pMNCs within iodinated oil induced significantly enhanced liver cancer cell death.

*Corresponding author. Department of Radiology, Seoul National University Hospital, Seoul, Korea. **Corresponding author. Department of Radiology, Northwestern University, Chicago, IL, USA.

[1]These authors contributed equally to this work.

1. INTRODUCTION

Interventional radiology is a medical specialty offering minimally invasive treatment for patients under image-guidance, and has been at the intersection of multiple research fields including drug delivery, ablative therapies, pharmacology, medical devices and medical imaging. Image-guided procedures have been actively pursued to treat unresectable primary liver cancer, hepatocellular carcinoma (HCC). Only 5–15% of HCC patients are suitable candidates for surgery due to the advanced stage of HCC at time of diagnosis.[1–4] No systemic chemotherapy has proven to be effective in HCC patients, except for the oral multi-kinase inhibitor Sorafenib in advanced stage patients with good liver function.[5, 6] Transcatheter arterial chemoembolization (TACE) under image-guidance using X-ray angiography has been performed as the primary option for unresectable HCC with an advanced stage. TACE utilizes the preferential blood supply of HCC derived from the hepatic artery (~95%), thereby allowing local chemotherapy and embolization with minimal damage to the surrounding healthy parenchyma (primarily supplied via portal vein).[6] Conventional TACE is performed with intra-arterial infusion of iodized oil mixed with chemotherapeutic agents such as Doxorubicin (Dox) or drug combinations such as Dox, cisplatin and mitomycin.[7] Lipiodol (Andre Guerbet, Aulnay-sous-Bois, France) is the iodized oil which has been most commonly used in TACE. However, many pharmacokinetic properties such as drug distribution and release rates remain uncertain. In order to overcome the limitations of iodized oil, non-absorbable drug-eluting beads (DEBs) which are composed of a hydrophilic, ionic polymer that can bind Dox via an ion exchange mechanism have been developed for TACE. This new type of embolic material permits a somewhat more sustained drug release into the tumor tissues.[8–12] However, these DEBs have not yet demonstrated significant improvements in treatment outcomes compared with conventional TACE using iodized oil. Thus, development of modern multifunctional drug carriers for catheter-directed procedures will be critically needed to improve therapeutic outcomes in HCC. Multifunctional drug carriers can be visible with MR or CT and load high doses of drugs in a reproducible manner for controlled elution over an extended period of time (current DEBs microspheres offer only a rapid burst release profile). Superior material properties and elution profiles of the multifunctional platform should also achieve reduced systemic exposures of the drugs to non-target area in transarterial delivery.[13, 14] The potential benefits of these drug delivery systems are considerable because a sustained release of chemotherapy over time could increase tumor cell kill by maintaining a more efficacious drug concentration within the targeted tissues. Among various multifunctional platforms, porous magnetic nanoclusters (pMNCs) can serve as drug carriers for TACE in HCC.[15–19] Their magnetic susceptibility enables MRI monitoring, tracking and quantification of delivery of these chemo-drug-loaded pMNCs to targeted tissues.[20–22] In the present study, we synthesized Dox loaded pMNCs (Dox-pMNCs) and characterized Dox drug release kinetics and MR contrast effects. Then, Dox-pMNCs were combined with iodinated oil as a possible translational form to mirror routine clinical practice (Dox-pMNCs combined with iodized oil) and delivered to liver tumors via hepatic artery in the rabbit liver tumor model. Deposition of every injected material to the targeted tumor was monitored by follow-up imaging, and its therapeutic efficacy was evaluated by histopathological analysis of the treated specimen.

2. Materials and Methods

2.1. Materials

Ferric chloride ($FeCl_3$), 25% ammonium hydroxide, diethylene glycol (DEG), sodium hydroxide and polyacrylic acid (PAA) were purchased from Sigma-Aldrich. Doxorubicin hydrochloride was purchased from LC Labs (Woburn, MA, USA). ferucarbotran (Resovist, Schering, Germany), Lipiodol (Andre Guerbet, Aulnay-sous-Bois, France), iopamidol (Isovue, Bracco Imaging, Italy) were used for imaging and *in vivo* experiments.

2.2 Preparation of pMNCs and Doxorubicin Loading

pMNCs were synthesized using a high temperature hydrolysis reaction.[23, 24] A NaOH/DEG solution was prepared by dissolving 2g of NaOH in diethylene glycol (DEG) (20 ml). The solution was heated to 120 °C for 30 mins under nitrogen, cooled, and kept at 70°C. A mixture of $FeCl_3$ (0.4 mmol), polyacrylic acid (PAA) (4 mmol), and DEG (17 ml) was heated to 220 °C in a N_2 atmosphere for 30 min with vigorous stirring to form a transparent solution. The prepared NaOH/DEG solution (2 ml) was injected into the solution. The resulting mixture was further heated for 1 h. The final products were washed with a mixture of Milli-Q water and ethanol 3 times and re-dispersed in Milli-Q water and dried in vacuum at 60 °C for 8h. Dox was loaded on the carboxylic porous magnetic nano-clusters by electrostatic adsorption and physical complexation processes of mixing in ethanol/water (volume ratio=1:1) mixture, centrifuge and drying adsorption. Dox (1 mg) was incubated with the carboxylic pMNCs (5 mg) in ethanol/MilliQ water (pH=~6.7) at room temperature for 24 hours. The Dox-pMNC was washed 3 times with 10 mL of Milli-Q water and permanent magnet, and dispersed in PBS (Phosphate Buffer Solution, pH 7.2).

2.3. Characterization of Samples

The morphology and size of the synthesized pMNCs were characterized using a transmission electronic microscope (TEM; FEI Tecnai Spirit G2). The magnetic properties of the samples were characterized with superconducting quantum interface device (SQUID, MPMS-XL, USA). The thermal behavior of pMNCs was investigated using a NETZSCH STA409 thermogravimetric analyzer at a heating rate of 10 °C/min to 800 °C in air. BET (Brauauer, Emmett and Teller) nitrogen adsorption-desorption was measured to determine the surface area of the samples using a Micromeritics Tristar 3000 volumetric adsorption analyzer. The mean particle size, size-distribution and zetapotential of the samples were investigated with dynamic light scattering (DLS) using a Zetasizer Nano-S (Malvern, Herrenberg, Germany) equipped with a 4 mW HeNe laser.

2.4. Drug Loading Efficiency and Release Studies

3 samples of Dox-pMNCs with Lipiodol (a volume ratio of 1:1.5 (particle solution:Lipiodol)), Dox-pMNCs (weight ratio 1:5 at Dox:pMNCs), and Dox with Lipiodol (volume ratio: 1:1.5, Dox: 1 mg) were prepared and compared for *in vitro* drug release behaviors. The loading amount of Dox in Dox-pMNCs was determined with characteristic excitation and emission wavelengths (λ_{ex}=480 nm and λ_{em}=550 nm) in a plate reader (SpectraMax M5, Molecular Devices, CA, USA). Drug elution studies were performed to

investigate Dox release kinetics at 37 °C. An aqueous sample solution (5 mg/ml;1 ml) was placed in a membrane bag (Spectra/Por MWCO 10,000, Spectrum, Los Angeles, CA, USA) and then immersed in 40 ml of PBS solution. The temperature of the medium was maintained at 37 °C using a water bath. At specific time intervals, PBS medium (1 ml) was extracted and replaced with fresh medium. Concentrations of released Dox were determined using a plate reader (λ_{ex}=480 nm and λ_{em}=550 nm). These measurements were performed three times and averaged to determine percentages of cumulative drug release amounts over time.

2.5. Characterization of MR Relaxivity Properties

T2 relaxation times for the pMNCs were determined and compared with ferucarbotran (Resovist, Schering, Germany) using a 3 Tesla MRI scanner (Tim Trio, Siemens Healthcare, Erlangen, Germany). Imaging phantoms were prepared by diluting samples in 1% agarose at various concentrations of samples. The atomic Fe concentrations of the stock solutions were determined using Inductively Coupled Plasma Spectroscopy (ICP-MS, Perkin Elmer, Waltham, MA, USA) and MRI signal changes were measured with increasing Fe concentrations of the pMNCs. For T2 measurement, a Carr-Purcell-Meiboom-Gill (CPMG) sequence of 6 echoes was used with TR3=31000ms and TE3=36.4~44.83ms with an echo interval of 6.4 ms. The T2 values were calculated using a least squares single exponential fitting model pixel by pixel and then averaging over the ROIs. For each concentration, we performed a linear fit between relaxation value and particle concentration with corresponding slope thus providing relaxivity estimate (Origin 7.0, Northampton, MA).

2.6. Preparation of Rabbit Liver Tumor Model

This study was approved by the institutional animal care and use committee. Adult New Zealand white rabbits (n=15) weighing 3.0 to 3.5 kg were maintained in rooms with a constant temperature (23 °C) and a 12-hour light/dark cycle. During all procedures, anesthesia was induced with an intramuscular injection of 5 mg/kg-body weight tiletamine-zolazepam (Zoletil 50; Virbac, Carros, France) and 2 mg/kg-body weight of 2% xylazine hydrochloride (Rompun; Bayer, Seoul, Republic of Korea). The VX2 carcinoma strain was maintained in the right hind limb of a carrier rabbit by deep intramuscular injection throughout the study.[25–28] Through a midline abdominal incision, the left lobe of the liver was exposed, and a small piece of tumor (1 mm^3) obtained from the hind limb tumor was directly implanted into the subcapsular liver parenchyma using a needle.[25–28]

2.7. Animal Groups

Tumor-bearing rabbits (n=15) were equally divided into three groups. Group A (n=5) underwent hepatic intra-arterial (IA) infusion of Dox-pMNCs with Lipiodol [total: 0.5 ml, 0.2 ml of Dox-pMNCs (0.2 mg Dox, 1.4 mg PMC) and 0.3 ml of Lipiodol)]. Group B (n=5) underwent IA hepatic injection of Dox-pMNCs [total: 0.5 ml, Dox-pMNCs (0.2 mg Dox, 1.4 mg pMNCs)] alone. After each treatment, these animals were scanned to monitor IA injected samples and tumors with MRI and CT for 14 days. The control group (n=5) underwent hepatic IA injection of Dox-Lipiodol [total: 0.5 ml, 0.2 ml of Dox-iopamidol (0.2 mg Dox, 0.2 ml iopamidol (Isovue, Bracco Imaging, Italy) and 0.3 ml of Lipiodol)] to

compare with Group A and B. Iopamidol, a contrast agent, is used to dissolve Dox instead of water in clinical practice.

2.8. Imaging Analysis

For each animal, MR scans were performed 3 times during the experimental period: at 0 (just before treatment), 7 and 14 days after the IA infusion procedure. A 3.0-T clinical MR scanner (Tim Trio; Siemens Healthcare, Erlangen, Germany) was used with a knee coil to improve SNR and spatial resolution. The animals were fixed on a board in a supine position, and an abdominal bandage was tightly applied to reduce any movement artifact. Axial T2-weighted turbo spin-echo (repetition time/echo time, 4100 milliseconds/150 milliseconds; echo train length, 14; section thickness, 3 mm; field of view, 130 × 130 mm; matrix, 512× 358; number of excitations, 2.0) and T2*-weighted gradient-echo (repetition time/echo time, 113 milliseconds/10 milliseconds; flip angle, 20 degrees; section thickness, 3 mm; field of view, 136×136 mm; matrix, 320 × 320; number of excitations, 10.0) images were acquired, and evaluated on an image archiving and communications workstation (m-view; Marotech, Seoul, Republic of Korea). The T2-weighted images were used to confirm tumor formation and to measure the maximal long diameters of the tumors. On the T2*-weighted images, signal decreases induced by pMNCs were measured. After measuring the signal intensity of the tumor and the back muscles on the same T2*-weighted imaging slice, the relative tumor-back muscle signal intensity ratios were calculated. CT scans were also performed right after the MR imaging at 0, 7 and 14 days after the IA infusion procedure. A multi-detector CT scanner (SOMATOM Definition, Siemens Medical Solutions, Forchheim, Germany) was used with the following parameters: detector configuration, 64X0.6 mm; rotation time, 0.5 seconds; pitch, 0.9; 120 kilovolt peak; 200 mA s; 1.5 mm of slice thickness with no gap; and matrix, 512X512.

2.9. Pathological Analysis (H&E, Prussian Blue and TUNEL analysis)

All animals were euthanized with an intravenous injection of a lethal amount (7–10 mL) of xylazine hydrochloride under deep anesthesia immediately after the last imaging study at day 14 post-infusion. The hepatic tumors were carefully dissected from the liver, and placed in a bottle containing 5% formalin for subsequent histopathological examination; hematoxylin and eosin staining for general inspection, Prussian blue staining to identify porous iron oxide magnetic nanoclusters, and terminal deoxynucleotidyl transferase dUTP nick end labeling (TUNEL) staining for tumor viability evaluation. The obtained histological slides were imaged with optical microscope and the tumor viability was evaluated using image analysis software (Image J, version 1.45s; National Institutes of Health, Bethesda, MD).

2.10. Statistical Analysis

A nonparametric analysis was conducted using the Kruskal-Wallis test to compare the signal intensity ratio of the tumor to the back muscles, and tumor apoptosis rate of the experimental groups. When positive results were encountered, the Mann-Whitney post hoc test was used for one-to-one group comparisons. The data processing and analysis were performed using Statistical Package for the Social Sciences version 16.0 (SPSS, Inc, an IBM

Company, Chicago, IL). We rejected the null hypotheses if the 2-tailed P values were less than 0.05.

3. Results

3.1. Characterization of pMNCs and Doxorubicin Loading/Release

As shown in Fig. 1a and b, ~55 nm magnetic nano-clusters generated by PAA binding agent were synthesized by hydrothermal procedure. Pores among small iron oxide nanoparticles (~5 nm) were characterized by TEM images. Thermogravimetric-differential scanning calorimetry (TG-DSC) curves of the sample showed presence of PAA with iron oxide nanoparticles (Fig. 1c). Below 100 °C, the weight loss was 58%, which should be attributed to the removal of surface-adsorbed water. The main exothermal peak was at 230 °C, corresponding to the decomposition of carboxyl groups uncoordinated on the magnetic nano-clusters. The minor exothermal peak at 280 °C was attributed to the decomposition of carboxyl groups coordinated on the surface and interface of magnetic nano-clusters. The corresponding weight loss of decomposition of carboxyl groups was about 7%. The other minor exothermal peak at 635 °C was attributed to the decomposition of PAA in the magnetic nano-clusters. The corresponding weight loss was approximately 2%. For verification of the surface area and porous structure of the iron oxide clusters, nitrogen adsorption-desorption isotherms were obtained (Fig. 1d). The magnetic nano-clusters showed a type-IV isotherm (Fig. 1d), which was characterized for a mesoporous structure. [29] The Brunauer-Emmett-Teller (BET) surface area of the magnetic nano-clusters was measured to be 8.3 m^2g^{-1}. A broad peak from 4 nm to 30 nm was found for the magnetic nano-clusters, corresponding to both small pores among the iron oxide nanoparticles within nanoclusters and mesopores which is the interspace area among the iron oxide nanoclusters (inset in Fig. 1d). Dox chemo-drug was loaded onto the pMNCs by electrostatic interaction between Dox and PAA in the pMNCs. Dox loading was confirmed with zetapotential changes of Dox-pMNCs complexes. By adding increasing amounts of Dox, the zetapotential values changed from negative (−40 mV) of PAA coated pMNCs to more positive values (+10~15 mV) (Fig. 1e). The Dox loading efficiency into the PAA coated pMNCs was 92%. The synthesized pMNCs showed high saturation magnetization values of 58 emu/g at room temperature and allowed MR T2 contrast effects. r2 relaxivity of the synthesized pMNCs measured in 3T MRI was r2=198.6 $mM^{-1}s^{-1}$, which was higher MR r2 relaxivity than ferucarbotran (r2=146.1 $mM^{-1}s^{-1}$) (Fig. 1f).

3.2. *In Vitro* Doxorubicin Release Study

The *in vitro* drug release behavior of Dox-pMNCs, Dox-pMNCs within Lipiodol and Dox within Lipiodol was compared (performed in triplicate for each preparation) (Fig. 2). Both Dox-pMNCs and Dox-pMNCs within Lipiodol released only 20~30% of initially loaded Dox amounts while 92% of Dox in the Dox-Lipiodol preparation was released relatively quickly within 100 hours (Fig. 2b).

3.3. In Vivo Intra-Arterial Delivery of Porous Magnetic Nanoclusters in Liver Tumor Model

Two weeks after tumor implantation, tumor growth was confirmed with MR just before IA infusion procedures (Fig. 3a). For hepatic IA infusion, an 18-gauge IV sheath was inserted

into the right auricular artery, through which a microcatheter was advanced to reach the common hepatic artery. Then, tumor location and tumor feeding artery were identified with hepatic arteriogram (Fig. 3b). The prepared 3 samples of Dox-pMNCs mixed with Lipiodol (Group A), Dox-pMNCs (Group B), and Dox mixed with Lipiodol (Control Group) were successfully injected through the catheter located within the left hepatic artery (Fig. 3 representative images from Group A). The distribution of infused Dox-pMNCs within tumor tissues was confirmed as negative contrast areas (signal reductions) within the tumor upon T2*-weighted MR scans (Fig. 3c). Both group A (Fig. 4a) and B (Fig. 4b) exhibited intratumoral signal decreases persisting at 7 and 14 days after IA delivery, however there was a significant difference observed between tumor-to-back muscle signal intensity ratios measured for these two groups. Group A resulted in higher levels of Dox-pMNCs uptake in the tumor than Group B. In Group A, the MR signal intensity of the tumor was maintained at significantly lower levels until day 14 after the IA delivery, which suggested an enhanced deposition of Dox-pMNCs in tumor tissues via co-delivery with Lipiodol (Fig. 4a and c). Prussian blue staining of tumor tissues histologically confirmed the retention of Dox-pMNCs which had blue spots in the tumor vasculature (Fig. 4d). On TUNEL staining to analyze the therapeutic effects, Group A displayed significantly higher apoptosis rate (74.1%) than Group B (56.2%) and Control Group (61.8%) with a *p*-value less than 0.05 (Fig. 5). Whereas, there was no significant difference observed in the tumor apoptosis rates between Group B and Control Group (P>0.05).

4. Discussion

HCC is a malignant tumor characterized by its high vascularity to induce rapid progression. TACE remains the standard treatment for advanced HCC patients who are not eligible for surgical resection or percutaneous tumor ablation. The principle of TACE is based on intra-arterial injection of chemotherapeutic drugs mixed with carriers directly through the arteries that preferentially feed the targeted tumors. However, local tumor control following TACE is achieved in only 15–60% of cases, and 5-year survival rates are ranged in 8–43%.[30] Novel drug delivery carriers for TACE are required for better drug release profile and to allow for multimodal imaging which enables the carriers to be visible on various imaging modalities simultaneously. Herein, we report the development of pMNCs, which carry a large payload of cargo within the pores and strong MRI contrast effects. As shown in Fig. 1, small iron oxide nanoparticles (~5 nm) were assembled into nano-clusters with a PAA binding agent. The highly porous space generated by clustering was filled with PAA containing abundant carboxylic, which has strong affinity to positively charged Dox. The Dox molecule contains an amino group with a pK of 8.6;[31] meanwhile, the pK for PAA carboxylic groups is equal to 4.8.[32] The interfacial interaction between the carboxylate groups on the pMNCs and the amine groups on the Dox drug molecules was demonstrated with zeta-potential changes. The mesopores and abundant carboxylic groups with PAA in the pMNCs enhanced the loading efficiency up to 92%. 34 wt% Dox could be loaded into the pMNCs. The cytotoxicity of pMNC was measured in Clon-9 hepatocyte cells by an MTT assay. The pMNCs were non-toxic with over 80% cell viability maintained at concentrations of up to 1 mg/ml. Prior to *in vivo* studies, two samples of Dox-pMNCs and Dox-pMNCs-Lipiodol mixtures were prepared as shown in Fig. 2a. Both of these pMNCs

preparations demonstrated sustained Dox drug release at slower rates than conventional Dox-Lipiodol preparation. Dox is one of the most widely used chemotherapeutic drugs for HCC treatment.[33] The mechanism of action of Dox is DNA intercalating and inhibition of topoisomerase II.[34] Thereby Dox has the ability to block DNA replication and induce apoptosis. However, the performance of Dox may be limited because both DNA and topoisomerase are primarily located in the cell nuclei and thus challenges may arise due to poor intracellular drug delivery.[35] Therefore, sustained Dox release to achieve critical concentrations for sufficient Dox penetration into nuclei is critical. Our results showed that sustained drug release from Dox-pMNCs (Fig. 2b) could potentially enhance anticancer performance of Dox by increasing exposure time of targeted tumors. In addition, the pMNCs demonstrated a strong response to an external magnetic field (when compared to individual nanoparticles) due to much higher magnetization per particle. The high magnetization value of the pMNCs, while maintaining superparamagnetic properties, presents an opportunity for superior MR contrast effects. Our synthesized pMNCs demonstrated 1.35 fold higher MR T2 contrast effects than ferucarbotran (about 60 nm carboxydextran coated single iron oxide nanoparticles).[36] Because liver MR imaging allows significantly higher diagnostic accuracy and sensitivity for the detection of HCC compared with CT,[37] the strong MR contrast effects of the pMNCs could play a valuable role in monitoring drug delivery and therapeutic outcomes.

For *in vivo* intra-arterial administration of pMNCs, Lipiodol was used with the Dox-pMNCs to enhance targeting delivery to liver tumors. Lipiodol is an iodinated derivative of poppy seed oil with iodine content of 38–40% w/v and has been shown to be selectively taken up and retained by primary liver tumors for a long period of time.[38–42] Thus, Dox mixed with Lipiodol has been commonly infused to maximize the drug concentration and exposure time of tumor tissues in TACE. However, rapid Dox release from the Dox-Lipiodol emulsion has limited therapeutic outcomes. We hypothesized that Dox-pMNCs mixed with Lipiodol could enhance anti-cancer therapeutic efficiency by (1) sustained Dox release from pMNCs and (2) tumor specific retention by Lipiodol when infused via the hepatic artery. The VX2 liver tumor model was selected for the experimental model because rabbits are large enough to enable IA procedures, and the blood supply of the VX2 liver tumor is similar to that of human HCC. Also, the tumor is easily detected by various radiological methods.[25] In our study, MRI confirmed liver tumor generation in each rabbit and IA infusion of Dox-pMNC preparation performed under X-ray arteriography guidance. Then, the selective accumulation of IA infused Dox-pMNCs or Dox-pMNCs within Lipiodol in tumor regions was readily detected with *in vivo* MRI and CT. Long-term MRI and CT monitoring for 14 days clearly showed the different intra-tumoral distributions of samples (Dox-pMNCs with Lipiodol or Dox-pMNCs alone) following IA administration. These MR and CT imaging capabilities should be valuable for refining IA procedures, determining amounts and patient-specific distributions of drug carrier, estimating therapeutic index, and ultimately optimizing therapy for each individual patient (retreatment or potentially reposition of catheter for improve tumor coverage).

Though nanosized Dox-pMNCs were initially well targeted to tumors via IA injection (Fig. 4a and d), the retention time of Dox-pMNCs was shorter than Dox-pMNCs within Lipiodol.

MR signal changes following IA Dox-pMNCs and Dox-pMNCs within Lipiodol administration was ~1.5 fold different at 7 days with this difference maintained at 14 days. This result indicates that Lipiodol significantly contributed to the retention of Dox-pMNCs. The selective retention of Dox-pMNCs with Lipiodol in liver tumors likely results from the "siphoning effect" of Lipiodol in tumor vessels[43], the electrostatic difference between Lipiodol and cancerous endothelia, transcapillary leakage and potentially membrane attachment of Lipiodol to tumor cells and pinocytosis of Lipiodol by tumor cells (as noted in prior studies) [42]. The higher uptake and longer retention of Dox-pMNCs administered with Lipiodol produced higher apoptosis levels in the treated tumors (Group A) when compared to IA Dox-pMNCs or Dox-Lipiodol administration (Fig. 5). These results suggest that the sustained release profile of Dox-pMNCs can be significantly potentiated by Lipiodol for increased retention. Finally, the multimodal imaging capabilities of the Dox-pMNCs (MRI) and Lipiodol (CT) complex are very promising for image-guided therapy.

5. Conclusion

These synthesized Dox-pMNCs permitted efficient drug loading, sustained release and *in vivo* MRI of intra-tumoral delivery. Combining pMNC with iodized oil allowed multi-modal imaging of transcatheter IA delivery to liver tumors according to a well-established clinically relevant TACE protocol along with improved therapeutic efficacy compared to conventional Dox/lipiodol preparation and/or Dox-pMNCs alone. The pMNC drug delivery platform offers the potential to improve clinical outcomes during catheter-directed loco-regional therapies for liver cancer.

Acknowledgments

This work was supported by Basic Research Grant from ACS (American Cancer Society, ACS 279148) and grants R01CA141047, R21CA173491, R21EB017986 and R21CA185274 from the National Cancer Institute and National Institute of Biomedical Imaging and Bioengineering, and a grant from the Korean Health Technology R&D Project, Ministry of Health & Welfare, Republic of Korea (HI12C1148). This work was supported by the Center for Translational Imaging at Northwestern University.

References

1. Geschwind JFH. Chemoembolization for hepatocellular carcinoma: Where does the truth lie? J Vasc Interv Radiol. 2002; 13:991–4. [PubMed: 12397119]
2. Bruix J, Castells A, Bosch J, Feu F, Fuster J, GarciaPagan JC, et al. Surgical resection of hepatocellular carcinoma in cirrhotic patients: Prognostic value of preoperative portal pressure. Gastroenterology. 1996; 111:1018–22. [PubMed: 8831597]
3. Bruix J, Llovet JM. Prognostic prediction and treatment strategy in hepatocellular carcinoma. Hepatology. 2002; 35:519–24. [PubMed: 11870363]
4. Llovet JM, Fuster J, Bruix J, Grp BCLC. Intention-to-treat analysis of surgical treatment for early hepatocellular carcinoma: Resection versus transplantation. Hepatology. 1999; 30:1434–40. [PubMed: 10573522]
5. Chen J, Sheu AY, Li W, Zhang Z, Kim DH, Lewandowski RJ, et al. Poly(lactide-co-glycolide) microspheres for MRI-monitored transcatheter delivery of sorafenib to liver tumors. J Control Release. 2014; 184:10–7. [PubMed: 24727059]
6. Kim DH, Chen J, Omary RA, Larson AC. MRI visible drug eluting magnetic microspheres for transcatheter intra-arterial delivery to liver tumors. Theranostics. 2015; 5:477–88. [PubMed: 25767615]

7. Liapi E, Geschwind JFH. Intra-Arterial Therapies for Hepatocellular Carcinoma: Where Do We Stand? Annals of surgical oncology. 2010; 17:1234–46. [PubMed: 20405328]
8. Liapi E, Lee K-H, Georgiades CC, Hong K, Geschwind J-FH. Drug-Eluting Particles for Interventional Pharmacology. Techniques in Vascular and Interventional Radiology. 2007; 10:261–9. [PubMed: 18572139]
9. Lewandowski RJ, Geschwind JF, Liapi E, Salem R. Transcatheter Intraarterial Therapies: Rationale and Overview. Radiology. 2011; 259:641–57. [PubMed: 21602502]
10. Lewis A, Gonzalez M, Leppard S, Brown J, Stratford P, Phillips G, et al. Doxorubicin eluting beads - 1: Effects of drug loading on bead characteristics and drug distribution. Journal of Materials Science: Materials in Medicine. 2007; 18:1691–9. [PubMed: 17483878]
11. Lewis AL, Gonzalez MV, Lloyd AW, Hall B, Tang Y, Willis SL, et al. DC bead: in vitro characterization of a drug-delivery device for transarterial chemoembolization. J Vasc Interv Radiol. 2006; 17:335–42. [PubMed: 16517780]
12. Liapi E, Geschwind JF. Intra-arterial therapies for hepatocellular carcinoma: where do we stand? Ann Surg Oncol. 2010; 17:1234–46. [PubMed: 20405328]
13. Varela M, Real MI, Burrel M, Forner A, Sala M, Brunet M, et al. Chemoembolization of hepatocellular carcinoma with drug eluting beads: efficacy and doxorubicin pharmacokinetics. Journal of hepatology. 2007; 46:474–81. [PubMed: 17239480]
14. Poon RT, Tso WK, Pang RW, Ng KK, Woo R, Tai KS, et al. A phase I/II trial of chemoembolization for hepatocellular carcinoma using a novel intra-arterial drug-eluting bead. Clinical gastroenterology and hepatology : the official clinical practice journal of the American Gastroenterological Association. 2007; 5:1100–8. [PubMed: 17627902]
15. Ai H, Flask C, Weinberg B, Shuai X, Pagel MD, Farrell D, et al. Magnetite-loaded polymeric micelles as ultrasensitive magnetic-resonance probes. Adv Mater. 2005; 17:1949-+.
16. Bastakoti BP, Hsu YC, Liao SH, Wu KCW, Inoue M, Yusa S, et al. Inorganic-Organic Hybrid Nanoparticles with Biocompatible Calcium Phosphate Thin Shells for Fluorescence Enhancement. Chem-Asian J. 2013; 8:1301–5. [PubMed: 23526653]
17. Wu KCW, Yang YH, Liang YH, Chen HY, Sung E, Yamauchi Y, et al. Facile Synthesis of Hollow Mesoporous Hydroxyapatite Nanoparticles for Intracellular Bio-imaging. Curr Nanosci. 2011; 7:926–31.
18. Yang YH, Liu CH, Liang YH, Lin FH, Wu KCW. Hollow mesoporous hydroxyapatite nanoparticles (hmHANPs) with enhanced drug loading and pH-responsive release properties for intracellular drug delivery. J Mater Chem B. 2013; 1:2447–50.
19. Liang YH, Liu CH, Liao SH, Lin YY, Tang HW, Liu SY, et al. Cosynthesis, of Cargo-Loaded Hydroxyapatite/Alginate Core-Shell Nanoparticles (HAP@Alg) as pH-Responsive Nanovehicles by a Pre-gel Method. Acs Appl Mater Inter. 2012; 4:6719–26.
20. Bromberg LE, Ron ES. Temperature-responsive gels and thermogelling polymer matrices for protein and peptide delivery. Adv Drug Deliver Rev. 1998; 31:197–221.
21. Da Silva RMP, Mano JF, Reis RL. Smart thermoresponsive coatings and surfaces for tissue engineering: switching cell-material boundaries. Trends Biotechnol. 2007; 25:577–83. [PubMed: 17997178]
22. Reed JA, Love SA, Lucero AE, Haynes CL, Canavan HE. Effect of Polymer Deposition Method on Thermoresponsive Polymer Films and Resulting Cellular Behavior. Langmuir. 2012; 28:2281–7. [PubMed: 21506526]
23. Ge JP, Hu YX, Biasini M, Beyermann WP, Yin YD. Superparamagnetic magnetite colloidal nanocrystal clusters. Angew Chem Int Edit. 2007; 46:4342–5.
24. Kim DH, Guo Y, Zhang Z, Procissi D, Nicolai J, Omary RA, et al. Temperature-sensitive magnetic drug carriers for concurrent gemcitabine chemohyperthermia. Advanced healthcare materials. 2014; 3:714–24. [PubMed: 24574255]
25. Kim KW, Lee JM, Kim JH, Klotz E, Kim HC, Han JK, et al. CT color mapping of the arterial enhancement fraction of VX2 carcinoma implanted in rabbit liver: comparison with perfusion CT. AJR American journal of roentgenology. 2011; 196:102–8. [PubMed: 21178053]

26. Kim YI, Chung JW, Park JH, Han JK, Hong JW, Chung H. Intraarterial gene delivery in rabbit hepatic tumors: transfection with nonviral vector by using iodized oil emulsion. Radiology. 2006; 240:771–7. [PubMed: 16857983]
27. Guo Y, Zhang Y, Jin N, Klein R, Nicolai J, Lewandowski RJ, et al. Electroporation-mediated transcatheter arterial chemoembolization in the rabbit VX2 liver tumor model. Investigative radiology. 2012; 47:116–20. [PubMed: 21934518]
28. Lee IJ, Ahn CH, Cha EJ, Chung IJ, Chung JW, Kim YI. Improved drug targeting to liver tumors after intra-arterial delivery using superparamagnetic iron oxide and iodized oil: preclinical study in a rabbit model. Investigative radiology. 2013; 48:826–33. [PubMed: 23835597]
29. Dong FP, Guo WP, Bae JH, Kim SH, Ha CS. Highly Porous, Water-Soluble, Superparamagnetic, and Biocompatible Magnetite Nanocrystal Clusters for Targeted Drug Delivery. Chem-Eur J. 2011; 17:12802–8. [PubMed: 21954062]
30. Vogl TJ, Zangos S, Balzer JO, Nabil M, Rao P, Eichler K, et al. Transarterial chemoembolization (TACE) in hepatocellular carcinoma: Technique, indication and results. Rofo-Fortschr Rontg. 2007; 179:1113–26.
31. Harrigan PR, Wong KF, Redelmeier TE, Wheeler JJ, Cullis PR. Accumulation of Doxorubicin and Other Lipophilic Amines into Large Unilamellar Vesicles in Response to Transmembrane Ph Gradients. Biochim Biophys Acta. 1993; 1149:329–38. [PubMed: 8323951]
32. Nagasawa M, Murase T, Kondo K. Potentiometric Titration of Stereoregular Polyelectrolytes. J Phys Chem-Us. 1965; 69:4005.
33. Lencioni R, de Baere T, Burrel M, Caridi JG, Lammer J, Malagari K, et al. Transcatheter treatment of hepatocellular carcinoma with Doxorubicin-loaded DC Bead (DEBDOX): technical recommendations. Cardiovascular and interventional radiology. 2012; 35:980–5. [PubMed: 22009576]
34. Pommier Y, Leo E, Zhang HL, Marchand C. DNA Topoisomerases and Their Poisoning by Anticancer and Antibacterial Drugs. Chem Biol. 2010; 17:421–33. [PubMed: 20534341]
35. Wang J, Ma L, Tang X, Zhang X, Qiao Y, Shi Y, et al. Doxorubicin induces apoptosis by targeting Madcam1 and AKT and inhibiting protein translation initiation in hepatocellular carcinoma cells. Oncotarget. 2015
36. Wang YX. Superparamagnetic iron oxide based MRI contrast agents: Current status of clinical application. Quantitative imaging in medicine and surgery. 2011; 1:35–40. [PubMed: 23256052]
37. Di Martino M, Marin D, Guerrisi A, Baski M, Galati F, Rossi M, et al. Intraindividual comparison of gadoxetate disodium-enhanced MR imaging and 64-section multidetector CT in the Detection of hepatocellular carcinoma in patients with cirrhosis. Radiology. 2010; 256:806–16. [PubMed: 20720069]
38. Konno T, Maeda H, Iwai K, Tashiro S, Maki S, Morinaga T, et al. Effect of arterial administration of high-molecular-weight anticancer agent SMANCS with lipid lymphographic agent on hepatoma: a preliminary report. European journal of cancer & clinical oncology. 1983; 19:1053–65. [PubMed: 6311559]
39. Nakakuma K, Tashiro S, Hiraoka T, Uemura K, Konno T, Miyauchi Y, et al. Studies on anticancer treatment with an oily anticancer drug injected into the ligated feeding hepatic artery for liver cancer. Cancer. 1983; 52:2193–200. [PubMed: 6196102]
40. Bretagne JF, Raoul JL, Bourguet P, Duvauferrier R, Deugnier Y, Faroux R, et al. Hepatic artery injection of I-131-labeled lipiodol. Part II. Preliminary results of therapeutic use in patients with hepatocellular carcinoma and liver metastases. Radiology. 1988; 168:547–50. [PubMed: 2839867]
41. Kan Z, Sato M, Ivancev K, Uchida B, Hedgpeth P, Lunderquist A, et al. Distribution and effect of iodized poppyseed oil in the liver after hepatic artery embolization: experimental study in several animal species. Radiology. 1993; 186:861–6. [PubMed: 8381552]
42. Wu HP, Feng GS, Tian Y. Hepatic artery infusion of antisense oligodeoxynucleotide and lipiodol mixture transfect liver cancer in rats. World journal of gastroenterology : WJG. 2005; 11:2408–12. [PubMed: 15832409]
43. Butler M, Stecker K, Bennett CF. Cellular distribution of phosphorothioate oligodeoxynucleotides in normal rodent tissues. Laboratory investigation; a journal of technical methods and pathology. 1997; 77:379–88.

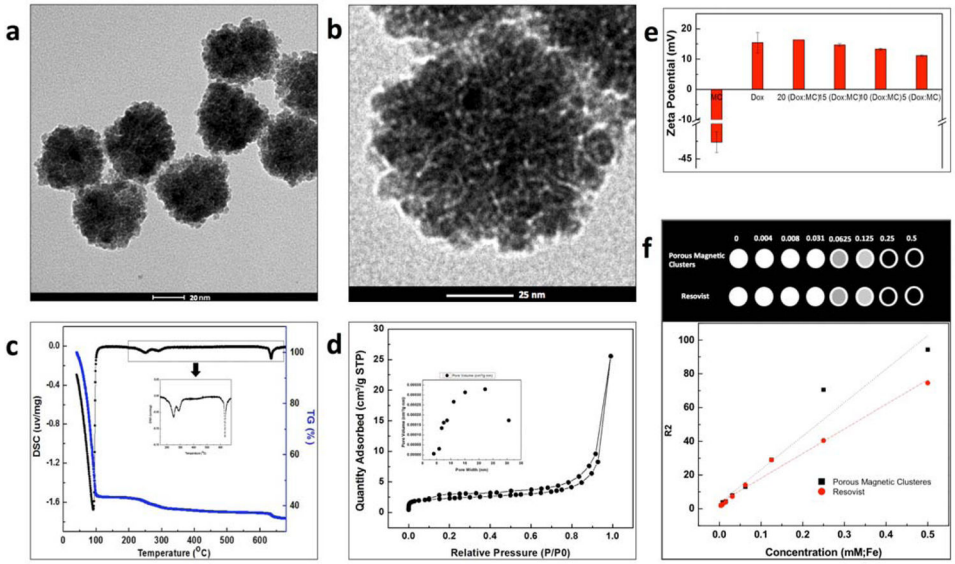

Fig. 1.

(a, b) TEM images of porous magnetic nanoclusters, (c) TG-DSC curves of porous magnetic nanoclusters showing surface adsorbed water and decomposition of carboxyl groups of PAA in the pMNCs, (d) BET nitrogen adsorption-desorption and (inset) pore size distribution of the pMNCs, (e) zeta potential changes of pMNCs in aqueous solution by increasing doxorubicin (Dox) loading amounts, and (f) T2-weighted MRI images (3T, spin-echo sequence) of various concentrations of pMNCs and ferucarbotran in agarose gel and T2 relaxation rates (1/T2, s^{-1}) as a function of iron concentration (mM) of pMNCs and ferucarbotran in agarose gel (3T, 25 °C).

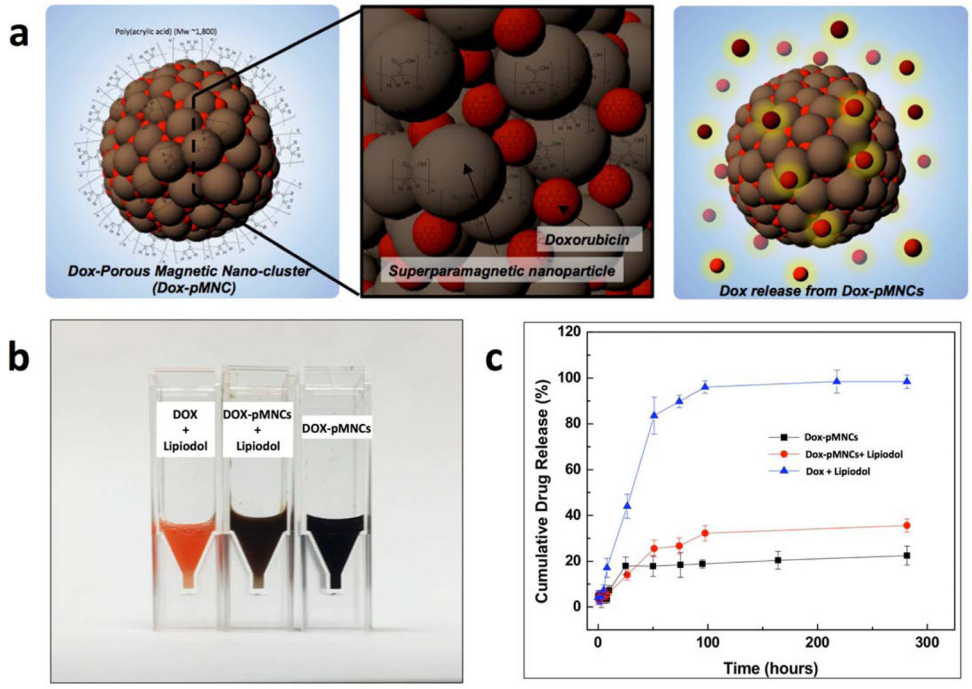

Fig. 2.

(a) Schematic illustration of Dox-loaded pMNCs for IA drug delivery, (b) digital image of sample solutions (Dox-pMNCs, Dox-pMNCs with Lipiodol and Dox with Lipiodol) and (b) Release profiles of Dox from the samples (Dox-pMNCs, Dox-pMNCs with Lipiodol and Dox with Lipiodol). The profiles of Dox-pMNCs and Dox-pMNCs with Lipiodol showed relatively slow and sustained drug release over 100 hours (at 37 ^{c}C).

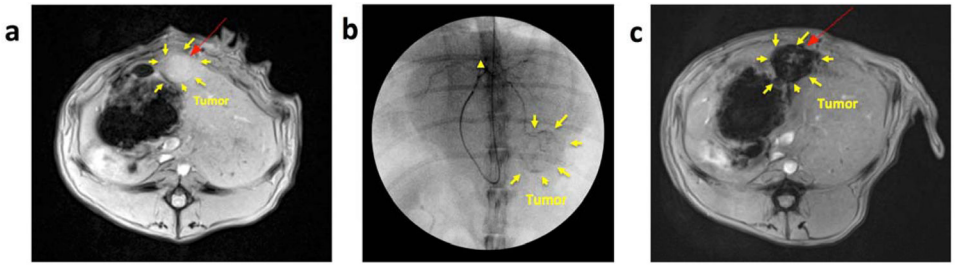

Fig. 3.

(a) MRI T2-weightd image of VX2 liver tumor in rabbit model before intra-arterial (IA) infusion procedure, (b) Digital subtraction angiography (DSA) during IA infusion of samples. A micro-catheter was advanced via the right ear artery, the descending thoracic aorta, and the celiac trunk, and the catheter tip was positioned at a feeder of the left hepatic artery (arrowhead). DSA during the IA infusion showed contrast agent opacification of the tumor tissues and feeding vessels (arrows indicate region of hypervascular tumor periphery). (c) MRI T2-weighted image of VX2 rabbit liver tumor after intra-arterial (IA) delivery of Dox-pMNCs with Lipiodol.

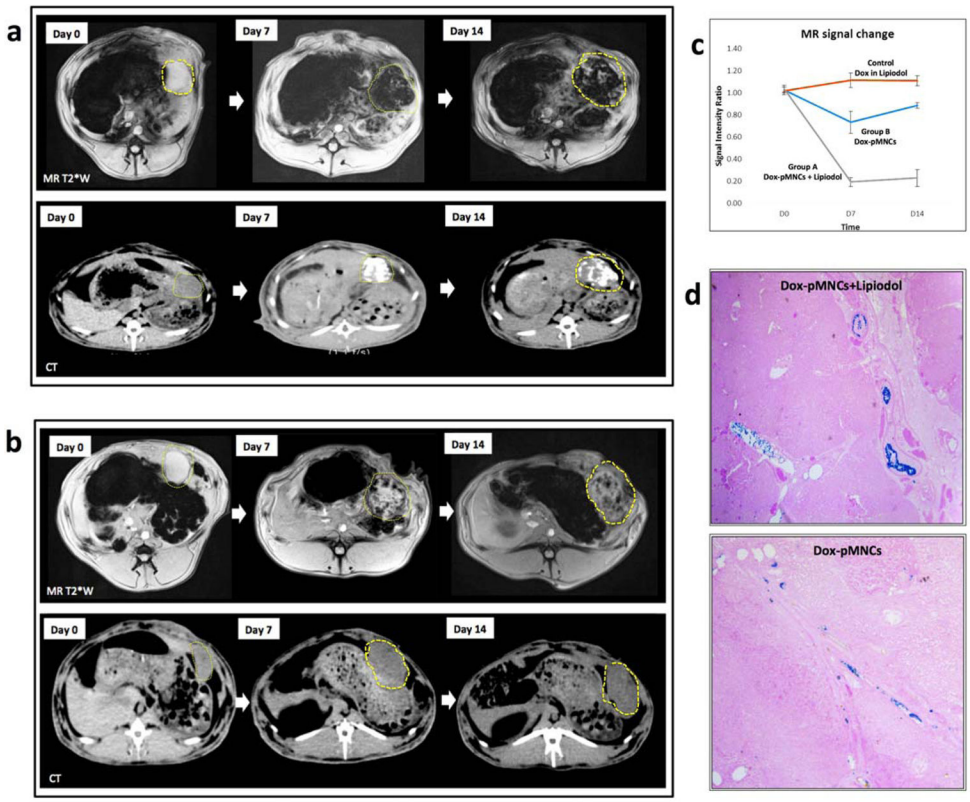

Fig. 4.

MRI T2* weighted images and CT images from (a) Group A rabbit (Dox-pMNCs with Lipiodol administered via IA infusion) and (b) Group B rabbit (Dox- pMNCs administered via IA infusion). In MR images before IA infusion, the tumor in the left hepatic lobe demonstrates high signal intensity (tumor position denoted with dashed-line ROI) in T2*-weighted images. At both days 7 and 14 after IA infusion, the tumor shows marked signal reduction in both Group A and B rabbits, due to deposition of the Dox-pMNCs in the tumor. CT images in Group A also showed dense Lipiodol deposits in the tumor at days 7 and 14 after the delivery. (c) Tumor-to-back muscle signal intensity ratios for the T2*-weighted images of Group A and B collected at 0, 7 and 14 days post-infusion. (d) Microscopic analysis (25×) of HCC tumor tissues harvested at 14 days and stained with Prussian blue. The iron in the deposits of the Dox-pMNCs was visible as a blue spots located at the inner edges of vascular structures.

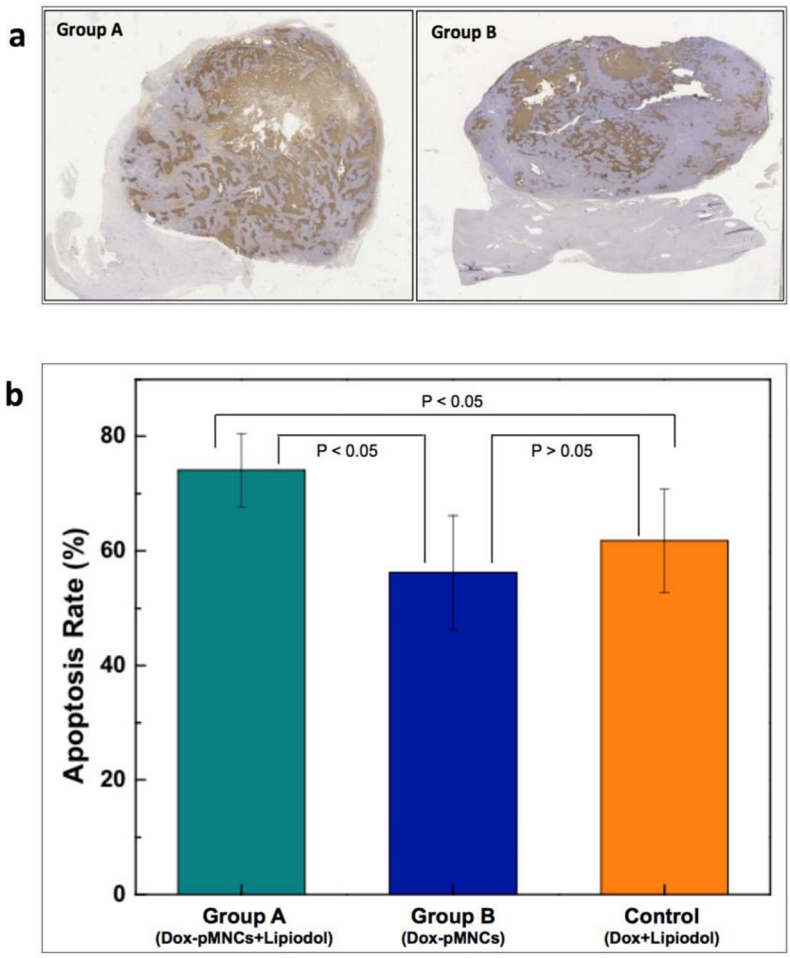

Fig. 5.

(a) Histological sections of VX2 liver tumors 14 days after treatment were TUNEL stained. The representative images from Group A and B rabbits are shown. Scattered positive cells were found study groups but a significant increase was observed for Group A (Dox-pMNCs within Lipiodol), and (b) quantitative analysis of TUNEL positive cells for Groups A, B and control. Data (means ± SD) represent the means of independent experiments (each n=5 in Group A and B, control). *p<0.05. (Group A and B). Increased TUNEL positive cells were observed in Group A vs. Group B and Group A vs. Control.